Published in final edited form as:
Nucl Med Biol. 2008 May ; 35(4): 447–458. doi:10.1016/j.nucmedbio.2008.02.009.

2-(2'-((Dimethylamino)methyl)-4'-(3-[^{18}F]fluoropropoxy)-phenylthio)benzenamine for PET Imaging of Serotonin Transporters

Julie L. Wang[1], **Ajit K. Parhi**[2], **Shunichi Oya**[2], **Brian Lieberman**[2], **Mei-Ping Kung**[2], and **Hank F. Kung**[1,2,*]

1*Department of Pharmacology, University of Pennsylvania School of Medicine, Philadelphia, PA 19104*

2*Department of Radiology, University of Pennsylvania School of Medicine, Philadelphia, PA 19104*

Abstract

Introduction—A new ^{18}F ligand, 2-(2'-((dimethylamino)methyl)-4'-(3-[^{18}F]fluoropropoxy)-phenylthio)benzenamine ([^{18}F]**1**), for positron emission tomography (PET) imaging of serotonin transporters (SERT) was evaluated.

Methods—Binding affinity was determined through *in vitro* binding assays with LLC-PK$_1$ cells overexpressing SERT, NET, or DAT (LLC-SERT, LLC-NET, and LLC-DAT) and with rat cortical homogenates. Localization and selectivity of [^{18}F]**1**_binding *in vivo* was evaluated by biodistribution, autoradiography, and A-PET imaging studies in rats.

Results—This compound displayed excellent binding affinity for SERT *in vitro* with K_i = 0.33 and 0.24 nM in LLC- SERT and rat cortical homogenates, respectively. Biodistribution studies with [^{18}F]**1** showed good brain uptake (1.61% dose/g at 2 min post-injection), high uptake into the hypothalamus (1.22% dose/g at 30 min), and a high target to non-target (hypothalamus to cerebellum) ratio of 9.66 at 180 min post-injection. Pretreatment with a SERT selective inhibitor considerably inhibited [^{18}F]**1**_binding in biodistribution studies. *Ex vivo* autoradiography reveals [^{18}F]**1** localization to brain regions with high SERT density, and this binding was blocked by pretreatment with SERT selective inhibitors. Small animal PET (A-PET) imaging in rats provided clear images of tracer localization in the thalamus, midbrain, and striatum. In A-PET chasing experiments, injecting a SERT selective inhibitor 75 min post-tracer injection causes a dramatic reduction in regional radioactivity and the target to non-target ratio.

Conclusion—The results of the biological studies and the ease of radiosynthesis with moderately good radiochemical yield (RCY = 10–35%) make [^{18}F]**1** an excellent candidate for SERT PET imaging.

Keywords

rat brain; autoradiography; binding affinity; 5-HTT; F-18; radioligand

*TO WHOM CORRESPONDENCE SHOULD BE ADDRESSED: Hank F. Kung, Ph.D., Department of Radiology, University of Pennsylvania School of Medicine, 3700 Market Street, Room 305, Philadelphia, PA 19104, Tel: (215) 662-3096, Fax: (215) 349-5035, e-mail: kunghf@gmail.com.

1. Introduction

Serotonin (5-HT) plays a regulatory role in many normal CNS and peripheral functions including sleep, appetite, memory, learning, temperature regulation, mood, sexual behavior, cardiovascular function, muscle contraction, and endocrine regulation [1]. It is widely accepted that lowered synaptic 5-HT levels correlate with disorders and disease states such as anxiety, bipolar disorder, obsessive compulsive disorder, schizophrenia, and depression [2,3]. In the brain, serotonin transporters (SERT) localized on 5-HT neurons serve as the main reuptake mechanism for terminating the action of 5-HT by transporting 5-HT from the synapse back into the presynaptic neuron. Selective serotonin reuptake inhibitors (SSRIs) bind to the serotonin transporter and effectively block the reuptake of serotonin into the synapse. Consequently, SSRIs are used in the treatment of depression as well as many other conditions. They are generally acknowledged to be the first-line therapy for depression, and they are one of the most commonly prescribed class of drugs in the world [4,5]. Although millions of patients with depression have benefited from SSRI treatment, a major drawback to this therapy is the 2–3 week lag before onset of clinical improvement, and at least 40% of patients fail to achieve a 50% reduction in depressive symptoms after a 6–8 week trial of SSRIs [6,7]. Response failure may be caused by several factors, but one of the most common factors is inadequate dosing [6]. As such, *in vivo* imaging of SERT radiotracers may be used to measure the effectiveness of antidepressant drug occupancy of SERT in the living human brain. Information gathered from these studies can be correlated with therapeutic efficacy and assist in the optimization of antidepressant drug dosing and therapy. In a broader scope, SERT can be used as a surrogate marker for serotonergic neuron integrity, and the ability to image SERT binding in the brain will expand our knowledge of normal functions and behaviors as well as various diseases and mental illnesses involving the serotonergic system.

Our goal is to develop an improved SERT radiotracer for use in positron emission tomography (PET). PET imaging has been useful in the study of the basic biology of the brain as well as diseases which afflict the brain, for instance, Alzheimer's and Parkinson's [8–12]. In these diseases various neurotransmitter and neuronal systems in the brain become altered. PET is a highly sensitive imaging technique, offering detection down to molar concentrations of 10^{-9} to 10^{-12}, that can been used for measuring the protein molecules involved in these systems, such as transporters, receptors, and enzymes, in the living human brain [12,13]. Molecular neuroimaging through PET is also relatively noninvasive, and it will be an important tool for the further understanding and treatment of various CNS diseases. In order for a ligand to be a good candidate for imaging SERT in the brain it should have high affinity and selectivity for SERT, moderate logP values within the range of 2 to 3.5 [14], high uptake and retention in SERT-rich brain regions, *in vivo* stability, and desirable *in vivo* kinetics including fast uptake and washout from the brain. Furthermore, ^{18}F labeled ligands for PET should have the capability of being radiolabeled quickly and efficiently. The first PET radiotracer successfully developed for imaging SERT density in the human brain was [^{11}C](+)McN5652. Although [^{11}C](+)McN5652 is able to successfully localize in SERT-rich regions of the brain, the nonspecific binding is relatively high resulting in a low target to non-target ratio and consequently, lower image resolution [15,16]. Attempts to find improved PET tracers led to the development of ^{11}C labeled DASB [17,18] (Table 1). [^{11}C]DASB is currently the ligand of choice, where ^{11}C tracers are made at a cyclotron in the near proximity, for imaging SERT [15]. Applications of [^{11}C]DASB in human PET studies have included investigating SERT binding in unmedicated patients with psychological disorders, central nervous system diseases, and alcoholism [19–21]. The feasibility of measuring drug occupancy of SERT by SSRIs *in vivo* using [^{11}C]DASB have also been reported [22–24].

A major drawback of [^{11}C]DASB, however, is that ^{11}C has a half-life of 20 min. The short half-life of ^{11}C labeled tracers limits their application to only medical centers possessing an

onsite cyclotron and skilled radiochemistry team. To address this shortcoming, significant efforts on preparation of various biphenylthiol derivatives have been made to develop PET SERT compounds that can be labeled with ^{18}F ($t_{1/2}$ = 110 min), such as DASB, AFM, ACF, and AFE (Table 1), but they have met with limited success [25–29]. To date, [^{18}F]FADAM is the most promising candidate [30]. However, the required nucleophilic substitution of ^{18}F on a less activated aromatic ring during radiolabeling results in a low radiochemical yield (< 5%) [31,32] thus making this tracer less practical for routine clinical use. To circumvent this low radiochemical yield in preparation of [^{18}F]FADAM, we have reported a novel series of SERT ligands with substituents at the 4'-position and 5-position of 2-(2'-((dimethylamino) methyl)-4'-(fluoroalkoxy)-phenylthio)benzenamine (Table 1)[33]. We maintained the biphenylthiol core structure because compounds in this class have previously demonstrated high affinity and selectivity for SERT, and its small size (molecular weight < 650 g/mole) facilitates passage through the blood brain barrier. Importantly, introduction of 4'- and 5-fluoroalkoxy substituents on the core structure provided a simple site for ^{18}F labeling, with labeled products obtained in comparatively high radiochemical yields. Furthermore, the 4'-fluoroalkoxy series indeed displayed high SERT affinity, *in vivo* selectivity, and excellent brain uptake after *iv* injection in rats. They also have appropriate lipophilicities and *in vivo* stability in the brain. Of the series, compounds **1** and **2** (Table 1) showed the most promise as SERT imaging agents [33]. Herein, we present data from biodistribution, autoradiography, and small animal PET (A-PET) imaging studies with [^{18}F]**1** in rats which have yielded favorable results and demonstrate the potential of employing this ligand for SERT imaging in conjunction with PET.

2. Materials and methods

2.1 General

Male Sprague-Dawley rats were used in the relevant studies. All protocols requiring the utilization of rats were reviewed and approved by the Institutional Animal Care and Use Committee (IACUC, University of Pennsylvania). Rats were put under isoflurane anesthesia prior to any injections, before sacrifice, and during the length of PET imaging. [^{125}I]NaI (0.1 N NaOH solution) was purchased from Perkin Elmer (Boston, MA, USA). Compound **1** and the corresponding mesylate precursor needed for the radiofluorination were prepared as reported previously [33]. IDAM was prepared as described previously [34]. (+)McN5652, Nisoxetine, GBR12909 were obtained from the NIMH chemical synthesis and drug supply program and Sigma-RBI (St. Louis, MO, USA). Escitalopram was kindly provided from Dr. Irwin Lucki (University of Pennsylvania).

2.2 Preparation of LLC-SERT, LLC-NET, and LLC-DAT membrane homogenates

Transfected LLC-PK_1 cell lines over-expressing a single monoamine transporter, the serotonin transporter (LLC-SERT), the norepinephrine transporter (LLC-NET), or the dopamine transporter (LLC-DAT) were kindly provided by Dr. G. Rudnick (Yale University) [35]. The parental LLC-PK_1 cell line was derived from pig renal epithelial cells which do not express SERT, NET, or DAT. Thus, the monoamine transport activity of LLC-SERT, LLC-NET, and LLC-DAT are due to the corresponding transfected DNA only. These cells were plated and grown to confluence with DMEM containing 10% FBS, 1x penicillin/streptomycin and 1 g/L G418, washed and harvested with PBS with 100 mg/mL calcium and 100 mg/mL magnesium (Gibco-Invitrogen), homogenized on ice with a Wheaton overhead stirrer, and centrifuged at 11,000 rpm for 20 minutes at 4 °C. The pellets were resuspended in the PBS buffer, frozen quickly in liquid N_2, and stored in a −80 °C freezer for future use in binding studies.

2.3 Preparation of rat cortical homogenates

The tissues of rat frontal cortex were dissected and homogenized in 20 times volume of 50 mM Tris buffer, pH 7.4, containing 120 mM NaCl and 5 mM KCl. The homogenates were centrifuged at 20,000 g for 20 min. The resulting pellets were resuspended in buffer and recentrifuged for 5 min. The final pellets were suspended in 5 times volume of buffer and used immediately for *in vitro* binding assays.

2.4 In vitro binding assays

For the SERT binding assays LLC-SERT membrane homogenates (100 μL corresponding to 30–50 μg protein) were mixed with 50 mM Tris-HCl, pH 7.4, 300 mM NaCl, 5 mM KCl and 1 mg/mL bovine serum albumin (BSA), the radioligand (0.1 nM [^{125}I]-IDAM, K_d = 0.09 nM), and a range of 10 concentrations (10^{-10} to 10^{-5} M) of the competing drug to be evaluated for a total volume of 0.5 mL. Nonspecific binding was defined with 2.5 μM (+)McN5652. Incubation was carried out for one hour at room temperature and then terminated by separation of bound from free radioligand by filtration through glass fiber filters presoaked with 1% polyethylenimine (Sigma, St. Louis, MO). The filters were then washed with cold 50 mM Tris-HCl, pH 7.4 buffer and counted in a gamma counter. Data analysis was performed using Microsoft Excel. The same procedures described above were used for the NET and DAT binding assays with the corresponding membrane homogenates (LLC-NET and LLC-DAT), radioligands (0.07 nM [^{125}I]2-INXT, K_d = 0.05 nM and 0.08 nM [^{125}I]IPT, K_d = 1.4 nM, respectively), and compound for non-specific binding determination (3.2 μM nisoxetine and 1.9 μM GBR12909, respectively) [36]. The same general procedures were followed when using rat cortical homogenates.

2.5 Radiochemistry

[^{18}F]**1** was prepared as reported previously (Fig. 1) [33]. Briefly, [^{18}F]Fluoride was produced by a JSW 3015 cyclotron at the Cyclotron Facilities at the University of Pennsylvania, or it was purchased from IBA Molecular North America Inc. (Sterling, VA) and passed through a Sep-Pak Light QMA cartridge. The ^{18}F activity was eluted with Kryptofix 222/K_2CO_3 / CH_3CN /H_2O solution, dried under an N_2 stream, and reacted with an O-mesylated precursor, 3-(3-((dimethylamino)methyl)-4-(2-nitrophenylthio)phenoxy)propyl methanesulfonate, in DMSO at 100 °C for 3 min. Water was added, and the mixture was passed through preconditioned Waters OASIS® HLB cartridge. The cartridge was washed with water, and the ^{18}F labeled nitro intermediate was eluted with ethanol. To this solution, 2N HCl and $SnCl_2$ were added, and the mixture was heated at 80 °C for 6 min. Water was added, and the mixture was passed through a preconditioned Waters OASIS® HLB cartridge. The cartridge was washed with water, and the desired ^{18}F labeled compound, [^{18}F]**1**, was eluted with CH_3CN and purified by semi-prep HPLC [Phenonemex Gemini C-18 semi-prep column (10 × 250 mm, 5 micron), CH_3CN/ ammonium formate buffer (50 mM) 55/45, flow rate 3 mL/min. t_R = 6 to 15 min]. Radiochemical purity and specific activity was calculated using analytical HPLC [Phenomenex Gemini C18 analytical column (4.6 × 250 mm, 5 micron), CH_3CN/ammonium formate buffer (10 mM) 8/2; Flow rate 1 mL/min; t_R = 4.0 to 6.5 min]. Specific activity was estimated by comparing UV peak intensity at 254 nm of purified [^{18}F] **1** with the reference non-radioactive compound of known concentration. At the end of synthesis, the radiochemical yield was 10–35% (decay corrected) with a radiochemical purity >97% and a specific activity of 320–6800 mCi/μmol. Chemical identification was confirmed by injection of the cold compound, **1**. Using the same HPLC conditions compound **1** showed the same retention time as that of [^{18}F]**1**.

2.6 Partition coefficient determination

To measure the partition coefficient, 3 g of 1-octanol and 3 g of 0.1 M NaH_2PO_4 buffer (pH 7.4) were added to roughly 1 million cpm of [^{18}F]**1** dissolved in < 10 μL of ethanol and vortexed for 1 min. The mixture was then centrifuged for 3 min. Samples of 2 mL each of the 1-octanol and buffer layers were weighed and then counted in a gamma counter. Additional 1-octanol was added to bring the 1-octanol fraction sample up to 3 g, and an additional 3 g of buffer was then added. The mixture was vortexed and centrifuged again as above. This procedure was repeated a total of 3 times. The partition coefficient was determined by calculating the ratio of cpm/mL of 1-octanol to that of buffer after the third partition.

2.7 Biodistribution in rats

While under isoflurane anesthesia, 40–100 μCi of [^{18}F]**1** dissolved in a small amount of ethanol (<5% of total volume of injection) and 0.2 mL of 1 mg/mL BSA solution was injected through the femoral vein. The rats were sacrificed under isoflurane at the time indicated (n=3 for each timepoint), and organs of interest were removed, weighed, and counted for radioactivity. The percent dose per organ was calculated by comparing the tissue counts to counts of 1% of the initial dose. The hypothalamus (HY), cortex (CX), striatum (ST), hippocampus (HP), and cerebellum (CB), were also dissected out of the brain, weighed, and counted to determine regional brain distribution. The percentage dose/g of each region was calculated by comparing sample counts with the counts of the diluted initial dose, as described above. It is known that high densities of SERT are located in the hypothalamus while intermediate densities are found in the hippocampus, intermediate levels in the striatum, and lower densities in the cortex [37–40]. Only a trace amount of SERT is present in the cerebellum, thus the cerebellum was used as the reference region for calculating the ratio of target to non-target binding. The ratio was calculated by dividing the percentage dose/g of each region by that of the cerebellum.

2.8 In vivo blocking/pharmacological specificity studies

A SERT, NET, or DAT selective inhibitor (2 mg/kg IDAM, 10 mg/kg nisoxetine, 2 mg/kg GBR, respectively) was first injected into the rat by the femoral vein. Nisoxetine was given at a dose of 10 mg/kg because of its relatively low brain uptake. The radiolabeled ligand (90 μCi) was then injected 5 min after the inhibitor. Regional brain distribution, as in the biodistribution studies described above, was determined 2 hr after injection of the radiolabeled ligand.

2.9 Ex vivo autoradiography of [^{18}F]1 in rat brain

Rats under isoflurane anesthesia were injected through the femoral vein with 0.2–0.5 mL of 1 mg/mL BSA solution containing 3.6–4.8 mCi of [^{18}F]**1**. At 60 min post-*iv* injection, the animals were sacrificed. The brains were removed, placed in embedding medium (Tissue Tek, Miles Laboratory, Elkhart, IN, USA) and frozen with powdered dry ice. After reaching equilibrium at −20 °C, consecutive 20 μm coronal sections were sliced on a cryostat microtome (Hacker Instruments, Fairfield, NJ, USA), thaw-mounted on microscope slides, and air-dried at room temperature. The slides containing the brain sections were exposed to film (Kodak BioMax MR) along with ^{125}I standards (Amersham Corp., Arlington, IL, USA) overnight in autoradiographic cassettes. To examine the specificity of [^{18}F]**1** for SERT, an injection of escitalopram (2 mg/kg) or nisoxetine (10 mg/kg) was given 5 min prior to [^{18}F]**1** injection.

2.10 PET imaging in rats

The radiotracer was dissolved in a small volume of ethanol (< 5% total volume of injection) and 1 mg/mL BSA solution. Approximately 1–1.4 mCi of radiotracer in a volume of 200–300 μL was injected through the tail vein. The specific activity varied from 652 mCi/μmol to 6800 mCi/μmol. Imaging was performed using the Philips Mosaic Animal PET (A-PET) imaging system [41,42] which has an image field of view of ~11.5 cm. Data acquisition commenced at

the time of [^{18}F]**1** injection. Scans were carried out over a period of 4 hrs taking 5 min per frame for the first 2 hrs and 15 min per frame for the last 2 hrs. Image voxel size was 0.5 mm^3. Region-of-interest analysis was performed using AMIDE (http://amide.sourceforge.net/) on reconstructed images. To examine the specificity of [^{18}F]**1** for SERT, an injection of escitalopram (2 mg/kg), IDAM (2 mg/kg), or nisoxetine (10 mg/kg) was delivered 75 min after [^{18}F]**1** injection.

3. Results

3.1 In Vitro Binding Assays

The binding affinity of nonradioactive compound **1** was evaluated using stably transfected LLC-PK$_1$ cell lines over-expressing SERT, NET or DAT (Table 1). Compound **1** displayed strong binding affinity to SERT ($K_{i,\ SERT}$ = 0.33 nM) and selectivity over DAT ($K_{i,\ DAT}$ = 299 nM). It is noted that some NET affinity was found ($K_{i,\ NET}$ = 11.9 nM). Since rat brain PET imaging was to be performed, binding affinity was further evaluated for native SERT and NET binding sites in the rat cortex (CX). DAT affinity in rat brain homogenates was not evaluated since compound **1** showed very low binding affinity for DAT in the LLC-DAT cell line. Results with cortical homogenates were comparable to the values determined in the cell lines ($K_{i,\ SERT,\ CX}$ = 0.24 nM and $K_{i,\ NET,\ CX}$ = 12.4 nM) giving ~50 fold selectivity for native SERT over native NET.

3.2 Biodistribution

To examine organ and regional brain biodistribution in rats, [^{18}F]**1** was injected through the femoral vein, and after selected timepoints, the rats were sacrificed. A critical requirement for a brain imaging agent is the ability to pass the blood brain barrier and to be taken up into the brain. Accordingly, [^{18}F]**1** showed high brain uptake at 2 min post *iv* injection. (Brain uptakes at 2, 30, 60, 120, 180, and 240 min were 1.61, 1.23, 0.97, 0.59, 0.30, and 0.24% dose/organ, respectively, Table 2). Various brain regions were dissected and counted to determine if brain uptake and retention of [^{18}F]**1** reflected regional distribution of SERT. Results showed high uptake in the hypothalamus, a SERT-rich region, as well as uptake in other SERT containing regions, namely the hippocampus, striatum, and cortex. With the cerebellum nearly devoid of SERT, it was used as the non-target region for calculating target to non-target ratios. High hypothalamus (HY) to cerebellum (CB) ratios were reached by 60 min (HY/CB = 4.69), and it steadily increased to 9.66 at 180 min while appearing to be maintained at 240 min. The relatively fast background washout of [^{18}F]**1** from the brain, i.e. fast and continual washout from the cerebellum, alongside retention in SERT localized regions resulted in the increase in target to non-target ratio over time and also indicated that [^{18}F]**1** may have desirable kinetic properties for imaging. Activity clearly dropped over a period of 240 min for all organs examined except for bone (Table 2). A relatively high amount of activity compared to other organs is still detected in the bone after 240 min. Although it is known that SERT is expressed in bone [43,44], it may be that [^{18}F]**1** undergoes some defluorination *in vivo*. The resulting free circulating fluoride may then have localized in the bone.

Pretreatment with selective monoamine transporter inhibitors demonstrated the SERT selectivity of [^{18}F]**1** *in vivo* in rats (Fig. 2). A two hour time-point was chosen for these pharmacological blocking biodistribution studies. Pretreatment with IDAM, a selective SERT inhibitor, greatly reduced regional brain uptake (i.e. 0.51 to 0.07% dose/g for the hypothalamus) and target to non-target ratios (i.e. 9.55 to 2.17 for HY/CB) when compared to control. Pretreatment with GBR12909 (DAT selective inhibitor) did not inhibit regional brain uptake or appreciably inhibit target to non-target ratios while pretreatment with nisoxetine (NET selective inhibitor) showed only minor inhibition.

3.3 Autoradiography

[^{18}F]**1** localized in brain regions containing medium to high SERT density (Fig. 3). At 60 min post-injection, [^{18}F]**1** prominently localized in the olfactory tubercles, thalamic nuclei, hypothalamic nuclei, substantia nigra, superior colliculus, dorsal raphe, medial raphe, and locus coeruleus (Fig. 3A). Pretreatment with the SERT selective inhibitor, escitalopram, effectively blocked [^{18}F]**1** localization to these regions with the exception of the locus coeruleus (Fig. 3B). There was some residual labeling in the hippocampus and lateral thalamic nuclei which may be due to non-specific binding of this ligand. Pretreatment with IDAM (2 mg/kg) showed similar results (data not shown). Pretreatment with nisoxetine failed to inhibit the [^{18}F]**1** binding seen in Fig. 3A with the exception of noticeably reduced binding in the locus coeruleus. The results suggested that the localization is specific for SERT; thus, we decided to proceed with animal PET imaging.

3.4 A-PET Imaging

A-PET imaging of rat brain showed clear [^{18}F]**1** localization in the thalamus, midbrain, and striatum (Fig. 4) which is consistent with the localization of SERT in the brain as determined by *ex vivo* autoradiography. Typical non-specific binding in the Harderian glands was also seen [45–47].

As predicted, there was minimal uptake in the cerebellum, and it was used as the non-target region in target to non-target ratio calculations. For image analysis, regions of interest (ROIs) (thalamus, midbrain, and striatum) were manually drawn to encompass only areas where high radioactivity was observable, since without an MR scan, it was difficult to consistently and precisely distinguish the boundaries of the different ROIs in the rat brain. Thus, the time activity curves (TACs) generated for the thalamus, midbrain, and striatum regions overlap (Fig. 5). As seen in the TACs generated from these images, [^{18}F]**1** uptake peaked at approximately 10–20 min (Fig. 5A**, left**) and steadily declined afterward showing fast washout. Region to cerebellum ratios peaked at 100–110 min (Fig. 5A**, right**) and also steadily declined afterwards. Injection of 2 mg/kg escitalopram 75 min post [^{18}F]**1** injection caused a marked drop in activity counts (Fig. 5B**, left**) as well as in region to cerebellum ratios (Fig. 5B**, right**). Similar results were seen with a 2 mg/kg IDAM injection (data not shown). An injection of 10 mg/kg nisoxetine at 75 min post [^{18}F]**1** injection did seem to cause some decrease in counts (Fig. 5C**, left**) and ratios (Fig. 5C**, right**) but not as dramatic a decrease as with an injection of escitalopram.

4. Discussion

Presently, [^{11}C]DASB is the preferred tracer for use in PET imaging of SERT in the living human brain. The short half-life of ^{11}C, however, limits routine use of this tracer to major medical centers that possess an on-site cyclotron and radiochemistry team. Hence, there is an urgent need to develop SERT ligands that can be conveniently labeled with a positron emitter with a longer half-life, ^{18}F. [^{18}F]FADAM is a promising candidate, but low radiochemical yield (< 5%) [31] due to difficult nucleophilic substitution of ^{18}F on an unactivated aromatic ring has made it less practical for routine use in clinical applications. As part of an effort to develop improved ^{18}F ligands prepared by easier radiolabeling steps for PET imaging of SERT binding sites in the brain, we had synthesized a novel series of biphenylthiols and examined their structure activity relationships [33]. They were designed to allow for greater ease in ^{18}F labeling and to achieve high radiochemical yield. Importantly, we were indeed able to obtain radiochemical yields of 10–35% with reasonable specific activity and high radiochemical purity within 70–90 min. This reaction can also be further optimized for a higher labeling yield and performed by an automated radiolabeling synthesizer commonly used in centralized radiopharmacies for making [^{18}F]FDG. Furthermore, SERT affinity and selectivity, and the ability to achieve good brain uptake were preserved. Two compounds of our series particularly

stood out. The 4'-(3-fluoropropoxy) (**1**) and 4'-(2-fluoroethoxy) analog (**2**) demonstrated strong affinity for SERT, suitable lipophilicities, high hypothalamus to cerebellum (target to non-target) ratios, and favorable *in vivo* kinetics as seen with fast brain uptake and comparatively fast brain washout yet good retention in the hypothalamus. Here we present a more in depth characterization of compound **1**.

The previously reported $K_{i,\ SERT}$ value for compound **1** in LLC-SERT cell homogenates was 1.44 nM [33]. Since then, we had determined the $K_{i,\ SERT}$ value in rat cortical homogenates and found it to be 0.24 nM. This difference prompted us to repeat the K_i, SERT determination in LLC-SERT cell homogenates, and we found it to be slightly lower at 0.33 nM. In rat biodistribution and blocking studies, treatment groups of n = 3 were utilized. It should be taken into consideration that three animals do not yield strong confidence in statistical analysis of the data set [48–50]. However, the studies give a good representation of the level of [^{18}F]**1** regional brain uptake achieved and the target to non-target ratios reached. Effects of SERT, NET, and DAT selective inhibitors on [^{18}F]**1** binding also give evidence to the selectivity of [^{18}F]**1** for SERT. The HY to CB ratio (target to non-target ratio) of [^{18}F]**1** reached 7.67 at 120 min, 9.66 at 180 min, and appeared to be maintained at 240 min post-injection. In comparison, the HY to CB ratio for [^{18}F]FADAM in rats has been reported in two separate papers to reach a high of 12.5 at 120 min post-injection [31] and a high of 7.5 at 90 min with a drop off to 4.2 at 120 min [26]. Along with a comparable HY to CB ratio, peak hypothalamus uptake of [^{18}F]**1** has also shown to be comparable with [^{18}F]FADAM, and the radiochemical yield has been significantly improved (10–35% vs. <5%).

A-PET imaging with [^{18}F]**1** in rats showed clear localization in the thalamus, hypothalamus, and striatum, regions known to contain SERT. Inhibitor chasing studies using A-PET were performed to further examine SERT binding specificity. An injection of the SERT selective inhibitor, escitalopram or IDAM, 75 min after [^{18}F]**1** injection clearly inhibited the tracer's binding immediately thereafter as evidenced by the dramatic drop in both activity and target to non-target ratios. In a separate inhibitor chasing study, we found that an injection of a NET selective inhibitor, nisoxetine, post [^{18}F]**1** injection also resulted in some inhibition of [^{18}F]**1** binding. We had considered this possibly occurring based on the binding affinities determined through the *in vitro* binding assays ($K_{i,\ SERT}$ = 0.33 and $K_{i,\ NET}$ = 11.9 nM in LLC-SERT and LLC-NET, respectively and $K_{i,\ SERT}$ = 0.24 and $K_{i,\ NET}$ = 12.4 nM in rat cortical homogenates). Compound **1** had displayed some NET affinity in these assays. Ideally, binding affinity for SERT would be 100 fold or greater than affinity for NET. However, *in vivo* biodistribution studies had shown that IDAM (a SERT selective ligand) considerably inhibits [^{18}F]**1** binding whereas nisoxetine (a NET selective ligand) had only minor inhibitory effects. Furthermore, *ex vivo* autoradiographs showed obvious inhibition of [^{18}F]**1** binding by IDAM or escitalopram pretreatment, whereas nisoxetine pretreatment did not. It was also reasoned that since the density of NET is at least four-fold less than the density of SERT in the brain [51], that compound **1** may be sufficiently selective for SERT. It is unclear why minimal inhibition was seen in the blocking biodistribution and autoradiograph studies where nisoxetine is injected 5 min before tracer injection, and a more prominent inhibition was seen in the A-PET imaging studies where nisoxetine is injected 75 min after tracer injection. Though some inhibition by nisoxetine was present in these A-PET studies, only escitalopram or IDAM was able to quickly and completely inhibit [^{18}F]**1** binding to cerebellar (background) levels. To further examine this issue, a dual SERT and NET inhibitor chasing experiment may be done to see whether the inhibitory effects would be significantly greater than escitalopram inhibition alone. This phenomenon of nisoxetine inhibition has been observed before by Ginovart et al. [22]. In PET experiments, they found that [^{11}C]DASB binding was inhibited 78–92% by a 2 mg/kg dose of nisoxetine in cats. However, they determined that another selective NET inhibitor, maprotiline, did not affect [^{11}C]DASB binding. They surmised that nisoxetine, a close structural analog of fluoxetine, may mediate the inhibition of [^{11}C]DASB binding directly or indirectly. They also

state that nisoxetine pretreatment did not affect [^{11}C]DASB binding in rats. One possible explanation for this is the dose used; they used a dose of 2 mg/kg whereas we used 10 mg/kg. Further validation of [^{18}F]**1** may be performed with PET imaging studies in non-human primates, such as monkeys or baboons. Co-registration of PET images with MR will accurately identify ROIs and facilitate quantification of regional brain distribution. In addition, more in depth kinetic modeling and metabolism studies shall be performed.

5. Conclusion

In conclusion, our results demonstrate the success of a novel ligand, [^{18}F]**1**, for small animal PET imaging of SERT binding sites in the brain. Furthermore, our studies highlight that this new probe possesses the desired qualities as an *in vivo* PET imaging agent for SERT: high SERT binding affinity, good brain uptake, selective regional brain localization, high target to non-target ratios, favorable kinetics, and ease of radiolabeling with relatively good radiochemical yield.

ACKNOWLEDGEMENTS

This work was supported by a grant awarded from the National Institutes of Health (ROI-MH068782, H.F.K.). Transfected LLC-PK$_1$ cell lines over expressing either SERT, NET or DAT were kindly provided by Dr. G. Rudnick of Yale University. NIMH chemical synthesis and drug supply program has provided several useful ligands ((+) McN5652, Nisoxetine, GBR12909). We are grateful to Eric Blankemeyer (Small Animal Imaging Facility, University of Pennsylvania), Catherine Hou and Brian Lieberman for their technical expertise and Ann-Marie Chacko for her editorial assistance in the preparation of this manuscript.

REFERENCES

1. Siegel, GJ. Basic Neurochemistry: Molecular, Cellular and Medical Aspects. Philadelphia: Lippincott Williams & Wilkins; 1999.
2. Kandel, ER.; Schwartz, JH.; Jessell, TM. Principles of Neural Science. McGraw-Hill Companies; 2000.
3. Schmitt JA, Wingen M, Ramaekers JG, Evers EA, Riedel WJ. Serotonin and human cognitive performance. Curr Pharm Des 2006;12:2473–2486. [PubMed: 16842171]
4. Fergusson D, Doucette S, Glass KC, Shapiro S, Healy D, Hebert P, Hutton B. Association between suicide attempts and selective serotonin reuptake inhibitors: systematic review of randomised controlled trials. BMJ 2005;330:396. [PubMed: 15718539]
5. Nemeroff CB. The burden of severe depression: A review of diagnostic challenges and treatment alternatives. J Psychiatr Res. 2006
6. DeBattista C, Solvason HB. When the first SSRI fails: a review of switching strategies in patients resistant to an initial SSRI. Essential Psychopharmacology 2003;5:217–224.
7. Frazer A, Morilak DA. What should animal models of depression model? Neurosci Biobehav Rev 2005;29:515–523. [PubMed: 15893377]
8. Maeda J, Ji B, Irie T, Tomiyama T, Maruyama M, Okauchi T, Staufenbiel M, Iwata N, Ono M, Saido TC, Suzuki K, Mori H, Higuchi M, Suhara T. Longitudinal, quantitative assessment of amyloid, neuroinflammation, and anti-amyloid treatment in a living mouse model of Alzheimer's disease enabled by positron emission tomography. J Neurosci 2007;27:10957–10968. [PubMed: 17928437]
9. Koerts J, Leenders KL, Koning M, Portman AT, van Beilen M. Striatal dopaminergic activity (FDOPA-PET) associated with cognitive items of a depression scale (MADRS) in Parkinson's disease. Eur J Neurosci 2007;25:3132–3136. [PubMed: 17561826]
10. Bohnen NI, Gedela S, Kuwabara H, Constantine GM, Mathis CA, Studenski SA, Moore RY. Selective hyposmia and nigrostriatal dopaminergic denervation in Parkinson's disease. J Neurol 2007;254:84–90. [PubMed: 17508142]
11. Swerdlow RH. PET sheds light on Alzheimer's disease genetic risk. Proc Natl Acad Sci U S A 2007;104:18881–18882. [PubMed: 18025455]
12. Hammoud DA, Hoffman JM, Pomper MG. Molecular neuroimaging: from conventional to emerging techniques. Radiology 2007;245:21–42. [PubMed: 17885179]

13. Wagner HN Jr. Molecular imaging: thriving all over the world. J Nucl Med 2007;48:15N–16N. 19N–38N. [PubMed: 17204694]

14. Waterhouse RN. Determination of lipophilicity and its use as a predictor of blood-brain barrier penetration of molecular imaging agents. Mol Imaging Biol 2003;5:376–389. [PubMed: 14667492]

15. Huang Y, Hwang DR, Narendran R, Sudo Y, Chatterjee R, Bae SA, Mawlawi O, Kegeles LS, Wilson AA, Kung HF, Laruelle M. Comparative evaluation in nonhuman primates of five PET radiotracers for imaging the serotonin transporters: [^{11}C]McN 5652, [^{11}C]ADAM, [^{11}C]DASB, [^{11}C]DAPA, and [^{11}C]AFM. J Cereb Blood Flow Metab 2002;22:1377–1398. [PubMed: 12439295]

16. Szabo Z, Scheffel U, Mathews WB, Ravert HT, Szabo K, Kraut M, Palmon S, Ricaurte GA, Dannals RF. Kinetic analysis of [^{11}C]McN5652: a serotonin transporter radioligand. J Cereb Blood Flow Metab 1999;19:967–981. [PubMed: 10478648]

17. Houle S, Ginovart N, Hussey D, Meyer JH, Wilson AA. Imaging the serotonin transporter with positron emission tomography: Initial human studies with [^{11}C]DAPP and [^{11}C]DASB. Eur J Nucl Med 2000;27:1719–1722. [PubMed: 11105830]

18. Wilson AA, Ginovart N, Hussey D, Meyer J, Houle S. In vitro and in vivo characterisation of [^{11}C]-DASB: a probe for in vivo measurements of the serotonin transporter by positron emission tomography. Nucl Med Biol 2002;29:509–515. [PubMed: 12088720]

19. Brown AK, George DT, Fujita M, Liow JS, Ichise M, Hibbeln J, Ghose S, Sangare J, Hommer D, Innis RB. PET [11C]DASB imaging of serotonin transporters in patients with alcoholism. Alcohol Clin Exp Res 2007;31:28–32. [PubMed: 17207098]

20. Cannon DM, Ichise M, Fromm SJ, Nugent AC, Rollis D, Gandhi SK, Klaver JM, Charney DS, Manji HK, Drevets WC. Serotonin transporter binding in bipolar disorder assessed using [11C]DASB and positron emission tomography. Biol Psychiatry 2006;60:207–217. [PubMed: 16875929]

21. Guttman M, Boileau I, Warsh J, Saint-Cyr JA, Ginovart N, McCluskey T, Houle S, Wilson A, Mundo E, Rusjan P, Meyer J, Kish SJ. Brain serotonin transporter binding in non-depressed patients with Parkinson's disease. Eur J Neurol 2007;14:523–528. [PubMed: 17437611]

22. Ginovart N, Wilson AA, Meyer JH, Hussey D, Houle S. [11C]-DASB, a tool for in vivo measurement of SSRI-induced occupancy of the serotonin transporter: PET characterization and evaluation in cats. Synapse 2003;47:123–133. [PubMed: 12454950]

23. Meyer JH, Wilson AA, Sagrati S, Hussey D, Carella A, Potter WZ, Ginovart N, Spencer EP, Cheok A, Houle S. Serotonin transporter occupancy of five selective serotonin reuptake inhibitors at different doses: an [11C]DASB positron emission tomography study. Am J Psychiatry 2004;161:826–835. [PubMed: 15121647]

24. Voineskos AN, Wilson AA, Boovariwala A, Sagrati S, Houle S, Rusjan P, Sokolov S, Spencer EP, Ginovart N, Meyer JH. Serotonin transporter occupancy of high-dose selective serotonin reuptake inhibitors during major depressive disorder measured with [11C]DASB positron emission tomography. Psychopharmacology (Berl) 2007;193:539–545. [PubMed: 17497139]

25. Garg S, Thopate SR, Minton RC, Black KW, Lynch AJ, Garg PK. 3-Amino-4-(2-((4-[18F] fluorobenzyl)methylamino)methylphenylsulfanyl)benzonitrile, an F-18 fluorobenzyl analogue of DASB: synthesis, in vitro binding, and in vivo biodistribution studies. Bioconjug Chem 2007;18:1612–1618. [PubMed: 17705553]

26. Huang Y, Bae SA, Zhu Z, Guo N, Roth BL, Laruelle M. Fluorinated diaryl sulfides as serotonin transporter ligands: synthesis, structure-activity relationship study, and in vivo evaluation of fluorine-18-labeled compounds as PET imaging agents. J Med Chem 2005;48:2559–2570. [PubMed: 15801845]

27. Huang Y, Hwang DR, Bae SA, Sudo Y, Guo N, Zhu Z, Narendran R, Laruelle M. A new positron emission tomography imaging agent for the serotonin transporter: synthesis, pharmacological characterization, and kinetic analysis of [11C]2-[2-(dimethylaminomethyl)phenylthio]-5-fluoromethylphenylamine ([11C]AFM). Nucl Med Biol 2004;31:543–556. [PubMed: 15219271]

28. Oya S, Choi SR, Coenen H, Kung HF. New PET Imaging Agent for the Serotonin Transporter: [^{18}F]ACF (2-[(2-Amino-4-chloro-5-fluorophenyl)thio]-N,N-dimethylbenzenmethanamine). J Med Chem 2002;45:4716–4723. [PubMed: 12361398]

29. Zhu Z, Guo N, Narendran R, Erritzoe D, Ekelund J, Hwang DR, Bae SA, Laruelle M, Huang Y. The new PET imaging agent [11C]AFE is a selective serotonin transporter ligand with fast brain uptake kinetics. Nucl Med Biol 2004;31:983–994. [PubMed: 15607480]
30. Huang, W.; Huang, S.; Yeh, C.; Ma, K.; Wang, H.; Peng, C.; Shiue, C. 18F-ADAM PET in healthy and drug-naive depressant subjects. Washington DC: 2007.
31. Shiue GG, Choi SR, Fang P, Hou C, Acton PD, Cardi C, Saffer JR, Greenberg JH, Karp JS, Kung HF, Shiue CY. N,N-dimethyl-2-(2-amino-4-(18)F-fluorophenylthio)-benzylamine (4-(18)F-ADAM): an improved PET radioligand for serotonin transporters. J Nucl Med 2003;44:1890–1897. [PubMed: 14660713]
32. Peng CJ, Huang YY, Huang WS, Shiue CY. An automated synthesis of N,N-dimethyl-2-(2-amino-4-[(18)F]fluorophenylthio)benzylamine (4-[(18)F]-ADAM) for imaging serotonin transporters. Appl Radiat Isot. 2007In Press
33. Parhi AK, Wang JL, Oya S, Choi SR, Kung MP, Kung HF. 2-(2′-((Dimethylamino)methyl)-4′-(fluoroalkoxy)-phenylthio)benzenamine Derivatives as Serotonin Transporter Imaging Agents. J Med Chem 2007;50:6673–6684. [PubMed: 18052090]
34. Oya S, Kung MP, Acton PD, Mu M, Hou C, Kung H. A new single-photon emission computed tomography imaging agent for serotonin transporters: [^{123}I] IDAM, 5-Iodo-2-((2-((dimethylamino) methyl)phenyl)thio)benzyl alcohol. J Med Chem 1999;42:333–335. [PubMed: 9986702]
35. Gu H, Wall SC, Rudnick G. Stable expression of biogenic amine transporters reveals differences in inhibitor sensitivity, kinetics, and ion dependence. J Biol Chem 1994;269:7124–7130. [PubMed: 8125921]
36. Kung MP, Hou C, Oya S, Mu M, Acton PD, Kung HF. Characterization of [^{123}I]IDAM as a novel single-photon emission tomography tracer for serotonin transporters. Eur J Nucl Med 1999;26:844–853. [PubMed: 10436197]
37. Choi SR, Hou C, Oya S, Mu M, Kung MP, Siciliano M, Acton PD, Kung HF. Selective in vitro and in vivo binding of [(125)I]ADAM to serotonin transporters in rat brain. Synapse 2000;38:403–412. [PubMed: 11044887]
38. Johnson MS, Lutz EM, Firbank S, Holland PJ, Mitchell R. Functional interactions between native Gs-coupled 5-HT receptors in HEK-293 cells and the heterologously expressed serotonin transporter. Cell Signal 2003;15:803–811. [PubMed: 12781873]
39. Kish SJ, Furukawa Y, Chang LJ, Tong J, Ginovart N, Wilson A, Houle S, Meyer JH. Regional distribution of serotonin transporter protein in postmortem human brain: is the cerebellum a SERT-free brain region? Nucl Med Biol 2005;32:123–128. [PubMed: 15721757]
40. Purselle DC, Nemeroff CB. Serotonin transporter: a potential substrate in the biology of suicide. Neuropsychopharmacology 2003;28:613–619. [PubMed: 12655305]
41. Surti S, Karp JS, Perkins AE, Cardi CA, Daube-Witherspoon ME, Kuhn A, Muehllehner G. Imaging performance of A-PET: a small animal PET camera. IEEE Trans Med Imaging 2005;24:844–852. [PubMed: 16011313]
42. Huisman MC, Reder S, Weber AW, Ziegler SI, Schwaiger M. Performance evaluation of the Philips MOSAIC small animal PET scanner. Eur J Nucl Med Mol Imaging 2007;34:532–540. [PubMed: 17119959]
43. Battaglino R, Fu J, Spate U, Ersoy U, Joe M, Sedaghat L, Stashenko P. Serotonin regulates osteoclast differentiation through its transporter. J Bone Miner Res 2004;19:1420–1431. [PubMed: 15312242]
44. Bliziotes MM, Eshleman AJ, Zhang XW, Wiren KM. Neurotransmitter action in osteoblasts: expression of a functional system for serotonin receptor activation and reuptake. Bone 2001;29:477–486. [PubMed: 11704501]
45. Kuge Y, Minematsu K, Hasegawa Y, Yamaguchi T, Mori H, Matsuura H, Hashimoto N, Miyake Y. Positron emission tomography for quantitative determination of glucose metabolism in normal and ischemic brains in rats: an insoluble problem by the Harderian glands. J Cereb Blood Flow Metab 1997;17:116–120. [PubMed: 8978394]
46. Thanos PK, Taintor NB, Alexoff D, Vaska P, Logan J, Grandy DK, Fang Y, Lee JH, Fowler JS, Volkow ND, Rubinstein M. In vivo comparative imaging of dopamine D2 knockout and wild-type mice with (11)C-raclopride and microPET. J Nucl Med 2002;43:1570–1577. [PubMed: 12411561]

47. Yang Y, Tai YC, Siegel S, Newport DF, Bai B, Li Q, Leahy RM, Cherry SR. Optimization and performance evaluation of the microPET II scanner for in vivo small-animal imaging. Phys Med Biol 2004;49:2527–2545. [PubMed: 15272672]

48. Eckelman WC. Further discussions on choosing the number of animals for an experiment. Nucl Med Biol 2008;35:1–2. [PubMed: 18158936]

49. Eckelman WC, Kilbourn MR, Joyal JL, Labiris R, Valliant JF. Justifying the number of animals for each experiment. Nucl Med Biol 2007;34:229–232. [PubMed: 17383571]

50. Scheibe PO. Number of samples - hypothesis testing. Nucl Med Biol 2008;35:3–9. [PubMed: 18158937]

51. Wilson AA, Patrick Johnson D, Mozley D, Hussey D, Ginovart N, Nobrega J, Garcia A, Meyer J, Houle S. Synthesis and in vivo evaluation of novel radiotracers for the in vivo imaging of the norepinephrine transporter. Nucl Med Biol 2003;30:85–92. [PubMed: 12623106]

52. Wilson AA, Ginovart N, Schmidt M, Meyer JH, Threlkeld PG, Houle S. Novel radiotracers for imaging the serotonin transporter by positron emission tomography: synthesis, radiosynthesis, and in vitro and ex vivo evaluation of ^{11}C-labeled 2-(phenylthio)araalkylamines. J Med Chem 2000;43:3103–3110. [PubMed: 10956218]

53. Oya S, Choi SR, Hou C, Mu M, Kung MP, Acton PD, Siciliano M, Kung HF. 2-((2-((Dimethylamino) methyl)phenyl)thio)-5-iodophenylamine (ADAM): An Improved Serotonin Transporter Ligand. Nucl Med Biol 2000;27:249–254. [PubMed: 10832081]

Abbreviations

1, 2-(2’-((dimethylamino)methyl)-4’-(3-fluoropropoxy)-phenylthio)benzenamine
2, 2-(2’-((dimethylamino)methyl)-4’-(2-fluoroethoxy)-phenylthio)benzenamine
PET, positron emission tomography
A-PET, animal positron emission tomography
SERT, serotonin transporter
DAT, dopamine transporter
NET, norepinephrine transporter
IDAM, (5-iodo-2-((2-(dimethylaminomethyl)-phenylthio)benzylalcohol)
5-HT, serotonin
(+)-McN5652, (+)-trans-1,2,3,5,6,10-beta-hexahydro-6-[4-(methylthio)phenyl]pyrrolo- [2,1-a]isoquinoline
DASB, 3-amino-4-(2-dimethylaminomethylphenylsulfanyl)benzonitrile
ADAM, 5-iodo-2’-(2-((dimethylamino)methyl)phenylthio)benzenamine
ACF, 2-[(2-amino-4-chloro- 5-fluorophenyl)thio]-N,N-dimethyl-benzenmethanamine
AFM, 2-[(2-amino-4-fluoro methylphenyl)thio]-N,N-dimethylbenzenemethanamine
AFE, 2-[2-[[(dimethylamino)methyl]phenyl]thio]-5-(2-fluoroethyl)phenylamine
FADAM, N,N-dimethyl-2-(2-amino-4-fluorophenylthio)benzylamine
nisoxetine, (±)-N-methyl-3-(2′-methoxyphenoxy)-3-phenylpropylamine
GBR12909, 1- (2-[bis(4-fluorophenyl)-[methoxy]ethyl)-4-(3-phenylpropyl) piperazine
2-INXT, (R)-N-methyl-(2-iodo-phenoxy)-3-phenylpropylamine
IPT, N-(3-iodopropen-2-yl)-2beta-carbomethoxy-3beta-(4-chlorophenyl) tropane
LLC-PK$_1$, Hampshire pig kidney cells
HY, hypothalamus
CX, cortex
ST, striatum
HP, hippocampus
CB, cerebellum
BSA, bovine serum albumin
ROI, region of interest
TAC, time activity curve

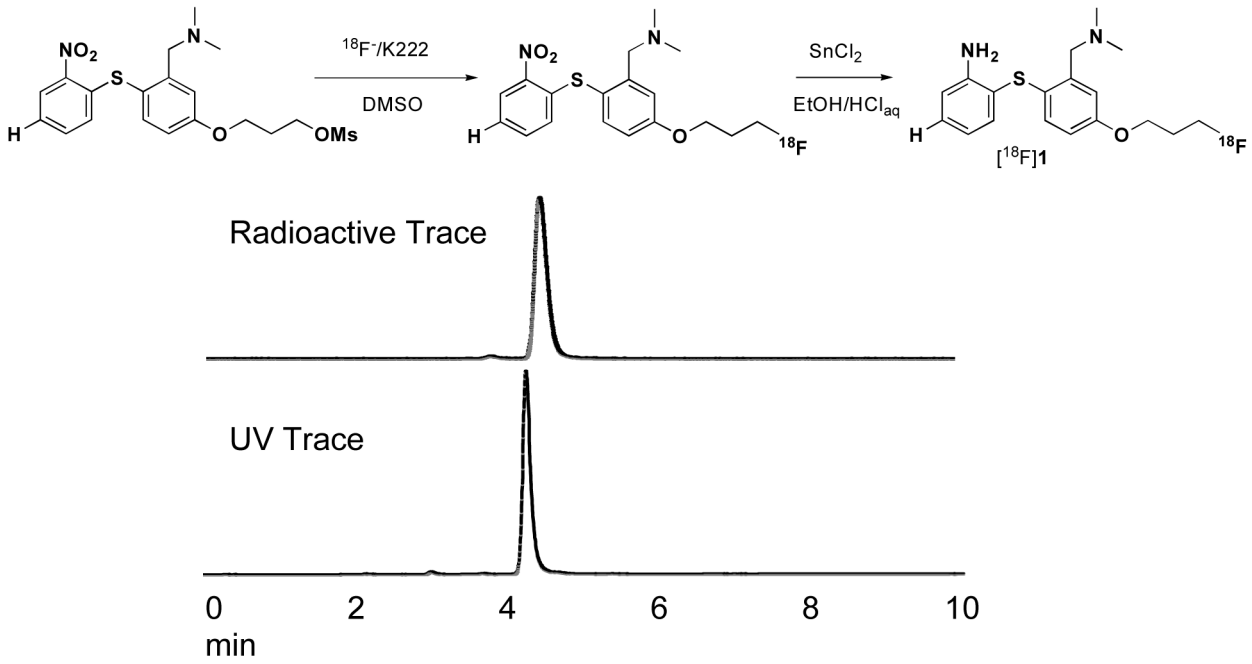

Figure 1.

HPLC traces of the purified product are shown above. Synthesis of [^{18}F]**1** was achieved by using a two step reaction with a radiochemical yield of 10–35%, radiochemical purity >97%, and specific activity of 320–6,800 mCi/μmol.

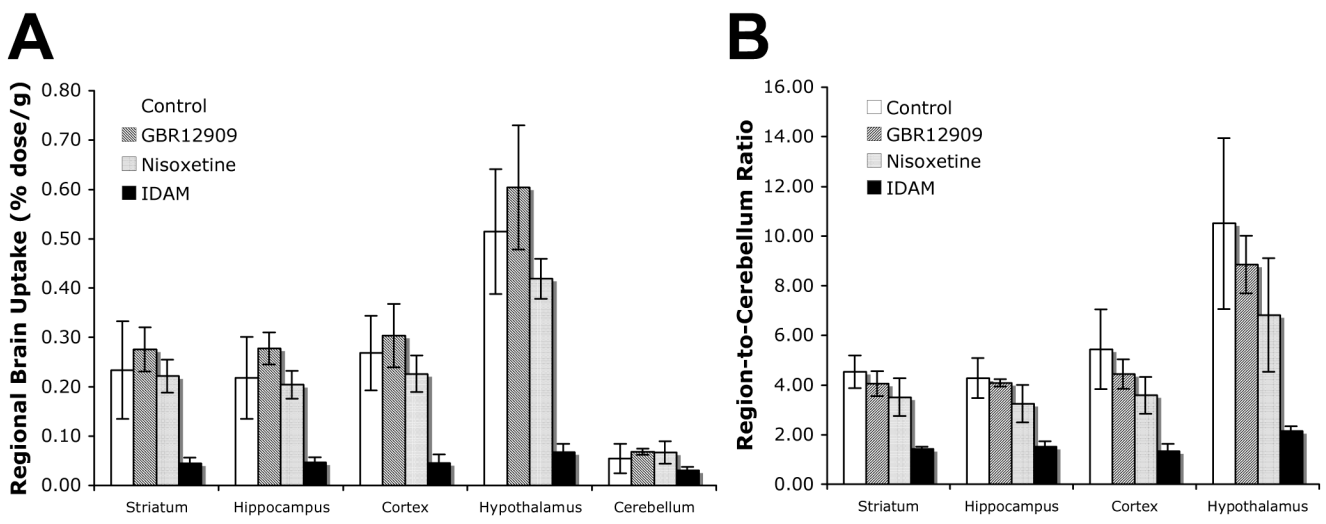

Figure 2.

The effects of pretreatment with selective monoamine transporter inhibitors on A: regional brain distribution and B: region-to-cerebellum ratios. While under isoflurane anesthesia, rats (n = 3) were injected with either sterile water, 2 mg/kg GBR12909 (selective DAT inhibitor), 10 mg/kg nisoxetine (selective NET inhibitor), or 2 mg/kg IDAM (selective SERT inhibitor) through the femoral vein 5 min before [^{18}F]**1** (90 μCi) injection. Two hours after tracer injection the tracer uptake in various brain regions were determined. Standard deviations are depicted by the error bars. **A:** IDAM considerably inhibits uptake into the striatum, hippocampus, cortex, and hypothalamus. **B:** Pretreatment with IDAM greatly decreased the region-to-cerebellum ratio. Negligible inhibition is seen with GBR12909, and minor inhibition is seen with nisoxetine pretreatment.

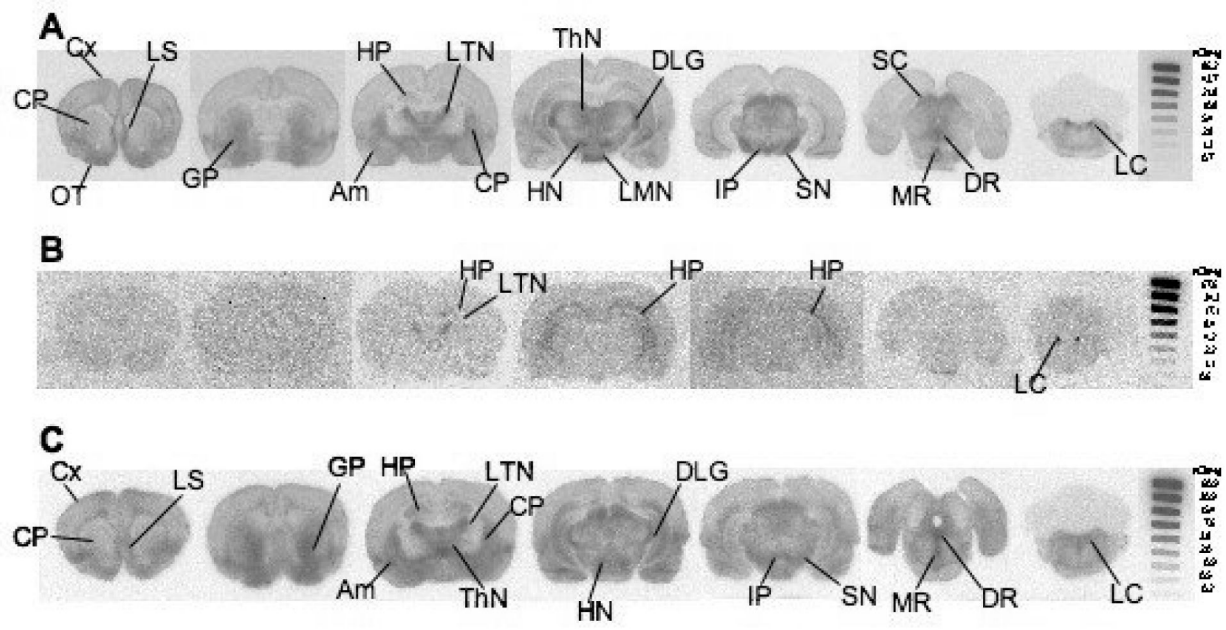

Figure 3.

Ex vivo autoradiograph shows [^{18}F]**1** localization in rat brain at 60 min post tracer injection. **A:** While under isoflurane anesthesia 3.6 mCi was injected through the femoral vein. Tracer localization is seen in regions with medium to high SERT density. **B:** Escitalopram (2mg/kg), a potent SERT inhibitor, was injected 5 min prior to [^{18}F]**1** (4 mCi) injection. Significant inhibition in regional brain uptake was observed in a rat pretreated with escitalopram. The results strongly suggest that [^{18}F]**1** and escitalopram compete for the same binding sites in the brain. Low amounts of non-SERT binding is seen in the HP, LTN, and LC. **C:** Nisoxetine (10 mg/kg), a selective NET inhibitor, was injected 5 min prior to [^{18}F]**1** (4.8 mCi) injection. Some inhibition in the locus coeruleus is seen, but otherwise [^{18}F]**1** localization is similar to that observed in **A**. The images suggest that [^{18}F]**1** is binding to SERT and not NET. An ^{125}I standard was exposed with each film to allow for a rough comparison between images generated from separate experiments. Cx: cortex; LS: lateral septum; OT: olfactory tubercle; CP: caudate putamen; GP: globus pallidus; HP: hippocampus; LTN: lateral thalamic nuclei; Am: amygdala; ThN: thalamic nuclei; DLG: dorsal lateral geniculate nucleus; LMN: lateral mammillary nuclei; HN: hypothalamic nuclei; IP: interpeduncular nucleus; SN: substantia nigra; SC: superior colliculus; DR: dorsal raphe; MR: medial raphe; LC: locus coeruleus.

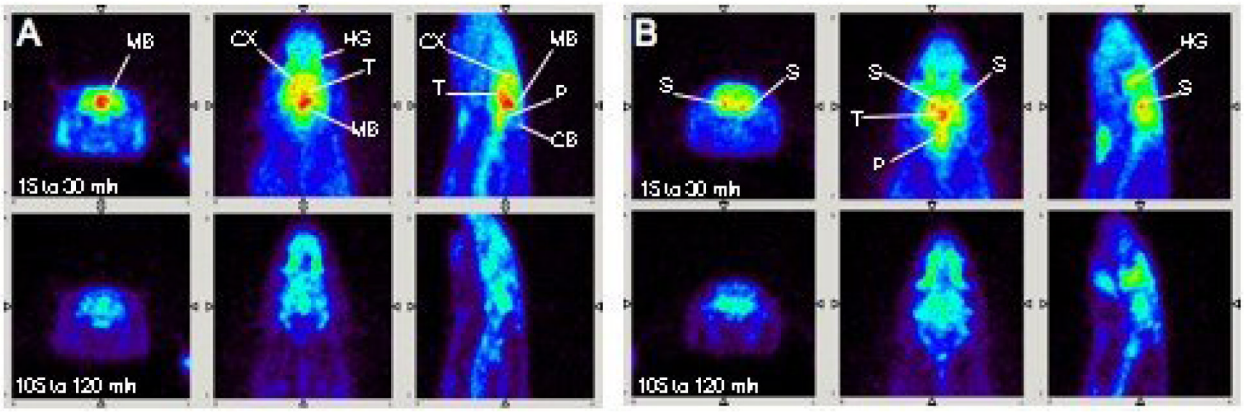

Figure 4.

While under isoflurane anesthesia, 1.2 mCi of [^{18}F]**1** was injected through a catheter placed into the tail vein and scanning commenced. A-PET images (coronal, transverse, and sagittal views shown) of [^{18}F]**1** localization in rat brain nicely reflect known areas of SERT distribution. Total scan time was four hours. Two time frames were selected to be shown here (15 to 30 and 105 to 120 min). **A:** [^{18}F]**1** localized in the midbrain (MB), cortex (CX), and thalamus (T) which are regions where SERT binding sites are concentrated. Activity due to non-specific binding was detected in the Harderian glands (HG); this non-specific binding is commonly observed in rats and mice for other PET agents [45–47]. Little uptake is seen in the cerebellum, a region with low SERT density. **B:** A different plane shows [^{18}F]**1** localization in another SERT-rich region, the striatum (S). A clear separation can be seen between the left and right striatum suggesting the usefulness of A-PET in imaging discrete structures in the brain.

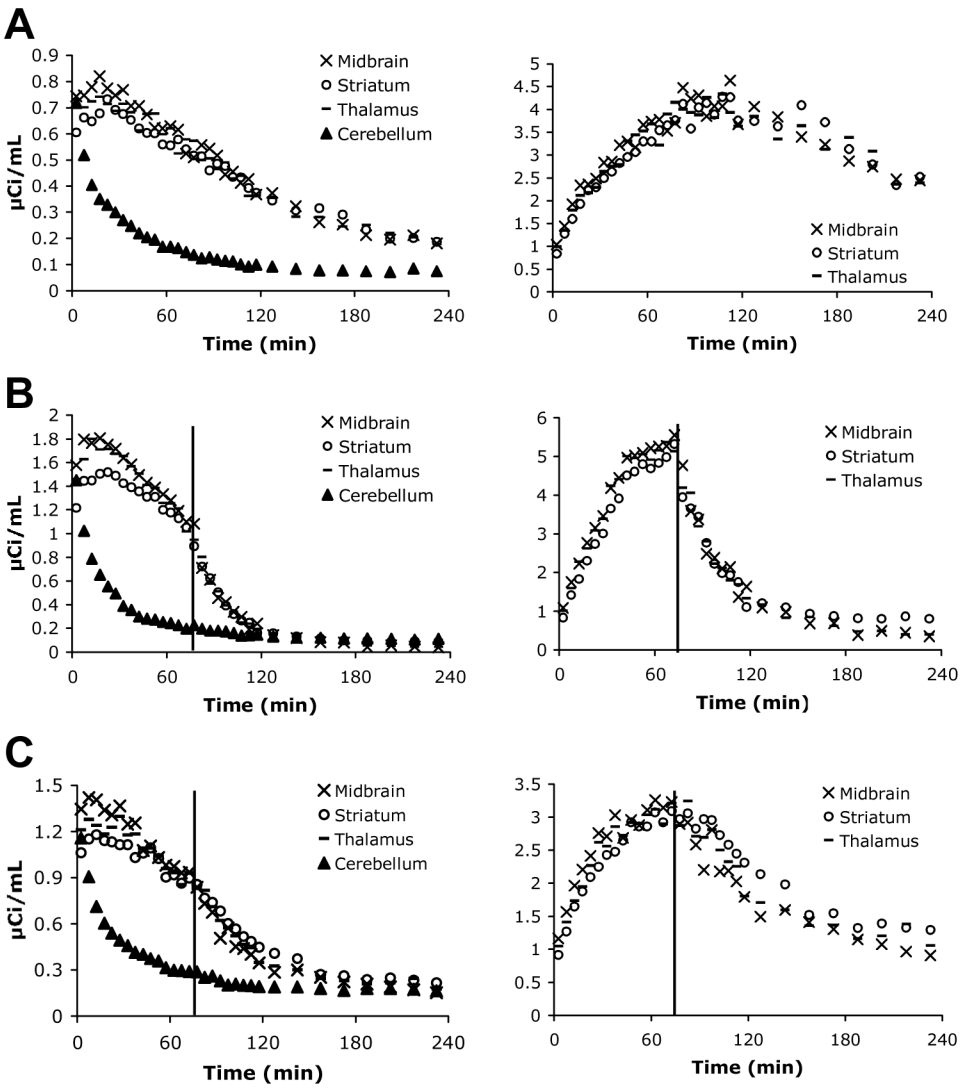

Figure 5.

Time activity curves were generated from A-PET image analysis using AMIDE software. Values on the y-axis for graphs A, C, and E represent μCi of activity detected per mL of brain. **A:** After a 1.17 mCi injection of [^{18}F]**1**, uptake peaked at 10–20 min, and activity counts in the non-target region, the cerebellum, dropped off quickly (left). The region-to-cerebellum ratio peaked at approximately 100–110 min (right). **B:** *IV* injection of escitalopram (2 mg/kg) 75 min after a 1.2 mCi injection of [^{18}F]**1** (indicated by red line) shows clear competition for SERT binding sites. Radioactivity in the target regions dropped off rapidly after escitalopram injection and reached cerebellar activity levels by 150 min (left). A dramatic drop in region-to-cerebellum ratio was also seen (right). Similar results were seen with a post-tracer injection of IDAM (data not shown). **C:** *IV* injection of the NET inhibitor, nisoxetine (10 mg/kg), after [^{18}F]**1** injection (1.43 mCi) also displayed inhibition of SERT binding; however, this could be a secondary effect. It remains to be evaluated further.

Table 1

Comparison of affinity (K_i, nM) and selectivity of compounds **1**, **2**, and previously reported ligands for the monoamine transporters expressed in cell lines or rat cortical tissue homogenates are shown below. Since low DAT affinity was found for compounds **1** and **2** through LLC-DAT binding assays, DAT binding in cortical homogenate was not further examined. The radioligands [^{125}I]-IDAM (K_d = 0.09 nM), [^{125}I]-INXT (K_d = 0.05 nM), and [^{125}I]-IPT (K_d = 1.4 nM) were used for determination of SERT, NET, and DAT affinity, respectively (n =3). LogP values determined at pH 7.4 are also shown.

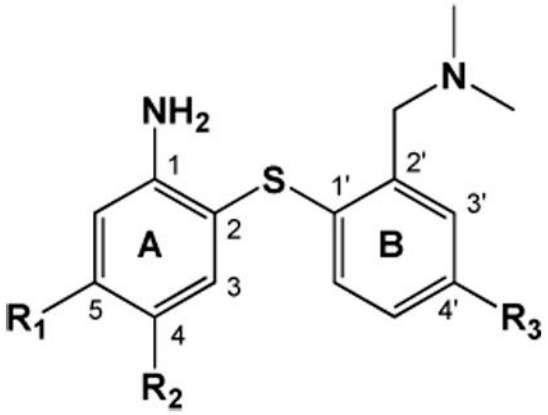

Compound	R_1	R_2	R_3	logP	$K_{i,SERT}$		$K_{i,NET}$		$K_{i,DAT}$
					Cloned SERT†	Rat Cortical	Cloned NET†	Rat Cortical	Cloned DAT†
DASB[a]	CN	H	H	2.7	1.10 ± 0.04	0.97 ± 0.07	1350 ± 221	6000 ± 760	1423 ± 103
ADAM[b]	I	H	H	2.5	0.01 ± 0.00	--	699 ± 80	--	840 ± 100
FADAM[c]	F	H	H	2.7	0.08 ± 0.01	--	117 ± 23	--	2267 ± 188
AFM[d]	CH_2F	H	H	--	1.04 ± 0.13	--	664 ± 80	--	>10,000
ACF[e]	Cl	F	H	--	0.05 ± 0.01	--	650 ± 80	--	3020 ± 110
AFE[f]	$(CH_2)_2F$	H	H	2.4	1.80 ± 0.07	--	946 ± 222	--	>10,000
1	H	H	$O(CH_2)_3F$	2.4	0.27 ± 0.01*	0.24 ± 0.07	11.9 ± 1.7	12.4 ± 2.0	299 ± 9
2	H	H	$O(CH_2)_2F$	2.1	0.25 ± 0.02	0.36 ± 0.03	7.53 ± 0.66	11.5 ± 1.4	340 ± 64

[a] [18,52]

[b] [53]

[c] [31]

[d] [27]

[e] [28]

[29]

†DASB with cloned human monoamine transporters; ADAM, FADAM, and ACF with LLC-PK1 cells expressing cloned human or rat monoamine transporters; AFM and AFE with HEK293 cells expressing cloned human monoamine transporters.

*The new K_i value is slightly lower from that reported previously (1.44 ± 0.22 nM) [33].

Table 2

Biodistribution of [^{18}F]**1** in male Sprague-Dawley rats (n = 3). While under isoflurane anesthesia, 40–100 μCi of [^{18}F]**1** was delivered by *iv* injection through the femoral vein.

Organ distribution in terms of % dose per organ

Region	2 min	30 min	60 min	120 min	180 min	240 min
Skin	7.72 ± 2.16	8.91 ± 1.39	9.75 ± 1.77	6.60 ± 0.67	3.86 ± 0.25	2.95 ± 0.24
Blood	6.95 ± 0.28	4.12 ± 0.41	3.30 ± 0.30	2.28 ± 0.54	1.21 ± 0.14	1.15 ± 0.08
Heart	0.90 ± 0.34	0.15 ± 0.03	0.10 ± 0.02	0.07 ± 0.01	0.04 ± 0.00	0.03 ± 0.01
Lung	10.1 ± 1.17	2.42 ± 0.31	1.45 ± 0.45	0.82 ± 0.15	0.47 ± 0.07	0.32 ± 0.00
Liver	6.27 ± 0.97	3.86 ± 0.20	3.43 ± 0.36	2.66 ± 0.70	2.37 ± 0.18	2.14 ± 0.32
Pancreas	0.78 ± 0.15	0.26 ± 0.00	0.17 ± 0.01	0.12 ± 0.03	0.05 ± 0.01	0.03 ± 0.01
Spleen	0.87 ± 0.09	0.61 ± 0.08	0.41 ± 0.08	0.19 ± 0.05	0.15 ± 0.02	0.09 ± 0.00
Kidney	6.00 ± 0.88	3.93 ± 0.58	3.59 ± 0.94	2.23 ± 0.80	2.34 ± 0.59	1.64 ± 0.81
Muscle	6.37 ± 0.26	9.94 ± 1.03	6.94 ± 1.36	4.48 ± 0.10	1.84 ± 0.16	1.42 ± 0.19
Bone	10.7 ± 1.47	8.79 ± 1.02	9.30 ± 1.00	8.84 ± 2.18	7.55 ± 0.33	8.83 ± 0.85
Brain	1.61 ± 0.02	1.23 ± 0.18	0.97 ± 0.18	0.59 ± 0.10	0.30 ± 0.01	0.24 ± 0.03

Regional brain distribution in terms of % dose per gram

Region	2 min	30 min	60 min	120 min	180 min	240 min
Hypothalamus	1.15 ± 0.11	1.22 ± 0.16	1.08 ± 0.21	0.75 ± 0.18	0.41 ± 0.02	0.34 ± 0.06
Striatum	0.92 ± 0.04	0.90 ± 0.17	0.74 ± 0.15	0.46 ± 0.10	0.16 ± 0.02	0.13 ± 0.00
Cortex	1.05 ± 0.07	1.00 ± 0.18	0.98 ± 0.18	0.44 ± 0.08	0.22 ± 0.09	0.12 ± 0.01
Hippocampus	0.89 ± 0.06	0.79 ± 0.11	0.65 ± 0.12	0.38 ± 0.04	0.20 ± 0.00	0.14 ± 0.02
Cerebellum	1.02 ± 0.11	0.35 ± 0.05	0.23 ± 0.07	0.10 ± 0.02	0.04 ± 0.00	0.03 ± 0.01

Region-to-cerebellum ratio calculated from % dose per gram values

Region	2 min	30 min	60 min	120 min	180 min	240 min
Hypothalamus	1.14 ± 0.15	3.50 ± 0.38	4.69 ± 0.74	7.67 ± 1.39	9.66 ± 0.21	10.1 ± 3.44
Striatum	0.90 ± 0.12	2.58 ± 0.30	3.19 ± 0.49	4.67 ± 0.29	3.88 ± 0.21	3.79 ± 0.64
Cortex	1.03 ± 0.12	2.87 ± 0.41	4.26 ± 0.96	4.53 ± 0.54	5.14 ± 1.87	3.64 ± 0.91
Hippocampus	0.88 ± 0.07	2.26 ± 0.25	2.82 ± 0.42	3.87 ± 0.50	4.65 ± 0.20	4.07 ± 0.88
Cerebellum	1.00 ± 0.00	1.00 ± 0.00	1.00 ± 0.00	1.00 ± 0.00	1.00 ± 0.00	1.00 ± 0.00